Three-Dimensional Upwind Parabolized Navier-Stokes Code for Real Gas Flows

John C. Tannehill,* Philip E. Buelow,† and John O. Ievalts†
Engineering Analysis, Inc., Ames, Iowa 50010
and
Scott L. Lawrence†
NASA Ames Research Center, Moffett Field, California 94035

A real gas, upwind, parabolized Navier-Stokes (PNS) code has been developed to compute the three-dimensional hypersonic flow of equilibrium air around various body shapes. The new code is an extension of the perfect gas, upwind PNS code (UPS code) of Lawrence, Tannehill, and Chaussee. The upwind algorithm is based on Roe's flux-difference splitting scheme, which has been modified to account for real-gas effects using the nearly exact approach of Vinokur and Liu. Simplified curve fits are employed to obtain the thermodynamic and transport properties of equilibrium air. The new code has been used to compute the $M_\infty = 25$ laminar flow of air over cones at various angles of attack. The results of these computations are compared with the results from a conventional centrally differenced, real-gas PNS code and the previous axisymmetric, upwind, real-gas code. The agreement is excellent in all cases. In addition, comparisons are made between results obtained using the approach of Vinokur and Liu, the approximate approach of Grossman and Walters, and the simple "effective gamma" approach.

Nomenclature

a = speed of sound
C_f = skin friction coefficient
C_h = heat transfer coefficient
E_t, e = total and internal energy, respectively
H, h = total and static enthalpy, respectively
J = Jacobian of transformation
k = total thermal conductivity
L = reference length, 1 m
M = Mach number, V/a
n = normal coordinate
Pr = Prandtl number
p = pressure
q_x, q_y, q_z = heat flux components
Re = Reynolds number, $\rho VL/\mu$
T = temperature
u, v, w = velocity components in x, y, z directions
V = total velocity
x, y, z = Cartesian coordinates or $y = y - y_{body}$
α = angle of attack
β = grid stretching parameter
γ = ratio of specific heats
$\bar{\gamma}$ = effective gamma (h/e)
κ = η or ζ coordinate
λ^i = ith eigenvalue
μ = coefficient of viscosity
ξ, η, ζ = transformed coordinates
ρ = density
τ_{ij} = shear stress
ϕ = circumferential angle
Δ = forward difference

Subscripts and Superscripts

i = inviscid part
m = index for κ coordinate
n, k, ℓ = indices in ξ, η, ζ directions
T = transpose
v = viscous part
w = wall
x, y, z = partial derivatives
∞ = freestream
$\tilde{}$ = dimensional quantity
$\hat{}$ = numerical approximation
$\bar{}$ = averaged quantity

Introduction

THE renewed interest in hypersonic aerothermodynamics has led to the development of several new parabolized Navier-Stokes (PNS) codes, which account for real-gas effects. These codes have been written for either equilibrium[1-8] or nonequilibrium[9-18] chemistry and have been applied to both two-dimensional and three-dimensional geometries. The majority of these codes are based on centrally differenced algorithms such as the Beam-Warming scheme.[19] One of the major drawbacks of this type of algorithm is that the central differencing of fluxes across flowfield discontinuities tends to introduce errors into the solution in the form of local flow property oscillations. To control these oscillations, some type of artificial dissipation is required. The correct magnitude of this added "smoothing" is generally left for the user to specify through some sort of "trial-and-error" process.

To overcome this difficulty, Lawrence et al.[20-21] have developed an upwind PNS code (UPS code), which is based on Roe's approximate Riemann solver.[22] The dissipation term associated with this scheme is sufficiently adaptive to flow conditions that, even when attempting to capture very strong shock waves, no additional "smoothing" is required. The superior shock capturing capability of this upwind PNS code has

Presented as Paper 89-1651 at the AIAA 24th Thermophysics Conference, Buffalo, New York, June 12-14, 1989; received June 30, 1989; revision received Aug. 19, 1989.

*President; currently Manager, Computational Fluid Dynamics Center, and Professor, Department of Aerospace Engineering, Iowa State University. Associate Fellow AIAA.
†Research Scientist. Member AIAA.

been demonstrated for both two-dimensional[20] and three-dimensional[21] perfect-gas flows. Recently, the two-dimensional version of the code was extended by the present authors to permit both equilibrium[23] and nonequilibrium[24] computations. The two-dimensional upwind algorithm was modified to account for real-gas effects using an approximate procedure, which was originally applied by Grossman and Walters[25] to a real-gas, upwind, time-dependent Euler code. Their procedure, which relies on the previous work of Colella and Glaz[26] was extended in Ref. 23 to the steady PNS equations. In addition, Balakrishnan and Lawrence[27] have recently applied a simple "effective gamma" approach to the three-dimensional UPS code to permit equilibrium air computations.

In the present work, the three-dimensional UPS code[21] has been further extended to permit real-gas computations using the approach of Vinokur and Liu.[28] The approach of Vinokur and Liu was adapted in the current study to the steady PNS equations. The resulting three-dimensional code has been used to compute the $M_\infty = 25$ laminar flow of equilibrium air over a 10-deg half-angle cone at various angles of attack. The results of these computations are compared with the results from the conventional, centrally differenced, real-gas PNS code of Prabhu et al.[3,12] and the previous two-dimensional/axisymmetric, upwind, real-gas PNS code.[23] In addition, comparisons are made between the approach of Vinokur and Liu, the approximate approach of Grossman and Walters, and the simple "effective gamma" approach. The three approaches are compared using a test case consisting of the $M_\infty = 30$ laminar flow of equilibrium air over a 20-deg half-angle cone at 0-deg angle of attack.

Governing Equations

The PNS equations are obtained from the compressible Navier-Stokes equations by dropping the unsteady terms and neglecting the stream-wise viscous derivatives in comparison with the normal viscous derivatives. The resulting equations, which are expressed in (ξ,η,ζ) computational coordinates via the generalized transformation

$$\xi = \xi(x,y,z), \qquad \eta = \eta(x,y,z), \qquad \zeta = \zeta(x,y,z)$$

can be written in nondimensional form[29] as

$$\frac{\partial \boldsymbol{E}}{\partial \xi} + \frac{\partial \boldsymbol{F}}{\partial \eta} + \frac{\partial \boldsymbol{G}}{\partial \zeta} = 0 \tag{1}$$

where

$$\boldsymbol{E} = (\xi_x/J)\boldsymbol{E}_i + (\xi_y/J)\boldsymbol{F}_i + (\xi_z/J)\boldsymbol{G}_i \tag{2a}$$

$$\boldsymbol{F} = (\eta_x/J)(\boldsymbol{E}_i - \boldsymbol{E}_v^*) + (\eta_y/J)(\boldsymbol{F}_i - \boldsymbol{F}_v^*) + (\eta_z/J)(\boldsymbol{G}_i - \boldsymbol{G}_v^*) \tag{2b}$$

$$\boldsymbol{G} = (\zeta_x/J)(\boldsymbol{E}_i - \boldsymbol{E}_v^*) + (\zeta_y/J)(\boldsymbol{F}_i - \boldsymbol{F}_v^*) + (\zeta_z/J)(\boldsymbol{G}_i - \boldsymbol{G}_v^*) \tag{2c}$$

The inviscid and viscous flux vectors are defined by

$$\boldsymbol{E}_i = [\rho u,\ \rho u^2 + p,\ \rho uv,\ \rho uw,\ (E_t + p)u]^T \tag{3a}$$

$$\boldsymbol{F}_i = [\rho v,\ \rho uv,\ \rho v^2 + p,\ \rho vw,\ (E_t + p)v]^T \tag{3b}$$

$$\boldsymbol{G}_i = [\rho w,\ \rho uw,\ \rho vw,\ \rho w^2 + p,\ (E_t + p)w]^T \tag{3c}$$

$$\boldsymbol{E}_v = [0,\ \tau_{xx},\ \tau_{xy},\ \tau_{xz},\ u\tau_{xx} + v\tau_{xy} + w\tau_{xz} - q_x]^T \tag{3d}$$

$$\boldsymbol{F}_v = [0,\ \tau_{xy},\ \tau_{yy},\ \tau_{yz},\ u\tau_{xy} + v\tau_{yy} + w\tau_{yz} - q_y]^T \tag{3e}$$

$$\boldsymbol{G}_v = [0,\ \tau_{xz},\ \tau_{yz},\ \tau_{zz},\ u\tau_{xz} + v\tau_{yz} + w\tau_{zz} - q_z]^T \tag{3f}$$

$$E_t = \rho[e + \tfrac{1}{2}(u^2 + v^2 + w^2)] \tag{3g}$$

The superscript asterisk on the viscous flux vectors in Eqs. (2) indicates that derivatives with respect to ξ have been eliminated. The equations have been nondimensionalized (dimensional quantities are denoted by a tilde) in the following manner:

$$\begin{aligned} x &= \tilde{x}/\tilde{L}, & u &= \tilde{u}/\tilde{V}_\infty, & \rho &= \tilde{\rho}/\tilde{\rho}_\infty & p &= \tilde{p}/\tilde{\rho}\tilde{V}_\infty^2 \\ y &= \tilde{y}/\tilde{L}, & v &= \tilde{v}/\tilde{V}_\infty, & T &= \tilde{T}/\tilde{T}_\infty, & e &= \tilde{e}/\tilde{V}_\infty^2 \\ z &= \tilde{z}/\tilde{L}, & w &= \tilde{w}/\tilde{V}_\infty, & \mu &= \tilde{\mu}/\tilde{\mu}_\infty, & k &= \tilde{k}/\tilde{k}_\infty \end{aligned} \tag{4}$$

To "close" the preceding system of PNS equations, relations between the thermodynamic variables are required along with expressions for the transport properties $\tilde{\mu}$ and $\tilde{k}$. For equilibrium air computations, approximate curve fits are employed for the thermodynamic and transport properties. The thermodynamic properties are obtained using the correlations

$$\begin{aligned} \tilde{p} &= \tilde{p}(\tilde{e},\tilde{\rho}), & \bar{\gamma} &= \bar{\gamma}(\tilde{e},\tilde{\rho}), & \tilde{a} &= \tilde{a}(\tilde{e},\tilde{\rho}) \\ \tilde{h} &= \tilde{h}(\tilde{p},\tilde{\rho}), & \tilde{T} &= \tilde{T}(\tilde{e},\tilde{\rho}), & \tilde{T} &= \tilde{T}(\tilde{p},\tilde{\rho}) \end{aligned} \tag{5}$$

developed by Srinivasan et al.[30] These curve fits are valid for temperatures up to 25,000 K and densities from 10^{-7} to 10^3 amagats ($\tilde{\rho}/\tilde{\rho}_0$). The pressure is computed using the expression

$$\tilde{p} = (\bar{\gamma} - 1)\tilde{\rho}\tilde{e} \tag{6}$$

where $\bar{\gamma}$ is defined by

$$\bar{\gamma} = \tilde{h}/\tilde{e} \tag{7}$$

For perfect-gas computations, $\bar{\gamma} = \gamma_\infty$. The curve fits for the transport properties were also developed by Srinivasan et al.[31] and include the following correlations

$$\tilde{\mu} = \tilde{\mu}(\tilde{e},\tilde{\rho}), \qquad \tilde{k} = \tilde{k}(\tilde{e},\tilde{\rho}) \tag{8}$$

The curve fits are based on the data of Peng and Pindroh[32] and are valid for temperatures up to 15,000 K and densities from 10^{-5} to 10^1 amagats. The use of the total thermal conductivity in the governing equations requires that the pressure gradient be negligible in the viscous layer.[33]

The PNS equations are a mixed set of hyperbolic-parabolic equations in the stream-wise direction ξ provided that the inviscid flow is supersonic, the stream-wise velocity component is everywhere greater than zero, and the stream-wise pressure gradient term in the stream-wise momentum equation is either omitted in subsonic regions or the "departure behavior" is suppressed by a suitable technique. In the present study, the technique of Vigneron et al.[34] is used to prevent departure solutions. The "Vigneron technique" involves splitting the $\boldsymbol{E}$ vector into two parts:

$$\boldsymbol{E} = \boldsymbol{E}^* + \boldsymbol{E}^P \tag{9}$$

where

$$\boldsymbol{E}^* = \begin{bmatrix} \rho\hat{U} \\ \rho u\hat{U} + (\xi_x/J)\omega p \\ \rho v\hat{U} + (\xi_y/J)\omega p \\ \rho w\hat{U} + (\xi_z/J)\omega p \\ (E_t + p)\hat{U} \end{bmatrix} \tag{10a}$$

$$\boldsymbol{E}^P = \begin{bmatrix} 0 \\ (\xi_x/J)(1-\omega)p \\ (\xi_y/J)(1-\omega)p \\ (\xi_z/J)(1-\omega)p \\ 0 \end{bmatrix} \tag{10b}$$

and

$$\hat{U} = (\xi_x/J)u + (\xi_y/J)v + (\xi_z/J)w \tag{11}$$

The $\boldsymbol{E}^*$ vector now replaces $\boldsymbol{E}$ in the numerical scheme, and $\boldsymbol{E}^P$ is neglected in the subsonic region. The final form of the governing equations becomes

$$\frac{\partial \boldsymbol{E}^*}{\partial \xi} + \frac{\partial \boldsymbol{E}^P}{\partial \xi} + \frac{\partial \boldsymbol{F}}{\partial \eta} + \frac{\partial \boldsymbol{G}}{\partial \zeta} = 0 \tag{12}$$

If $\boldsymbol{E}^P$ is neglected in the subsonic viscous region, an eigenvalue analysis for real-gas flows[3] shows that the PNS equations are hyperbolic-parabolic in the ξ direction provided that

$$\omega = \min\left[1, \frac{\sigma\bar{\gamma}M_\xi^2}{1 + (\bar{\gamma}-1)M_\xi^2}\right] \tag{13}$$

where M_ξ is the Mach number in the ξ direction, and σ is a safety factor that is included to provide for nonlinearities not accounted for in the analysis.

Numerical Method

The algorithm used in the present real-gas code is a modified version of the upwind, finite-volume algorithm developed by Lawrence et al.[21] to solve the (perfect gas) PNS equations. The upwind algorithm is based on Roe's scheme,[22] which has been modified in the present study for real-gas calculations.

The PNS equations can be written in discrete conservation-law form as

$$(\hat{E}_i)^{n+1}_{k,\ell} + (\hat{F}_i - \hat{F}^*_v)^{n+\frac{1}{2}}_{k+\frac{1}{2},\ell} + (\hat{G}_i - \hat{G}^*_v)^{n+\frac{1}{2}}_{k,\ell+\frac{1}{2}} - (\hat{E}_i)^n_{k,\ell}$$
$$- (\hat{F}_i - \hat{F}^*_v)^{n+\frac{1}{2}}_{k-\frac{1}{2},\ell} - (\hat{G}_i - \hat{G}^*_v)^{n+\frac{1}{2}}_{k,\ell-\frac{1}{2}} = 0 \tag{14}$$

where the accented vectors represent numerical approximations to the real fluxes at the sides of the finite volume over which conservation is desired. The forms of the numerical fluxes are similar to those given in Eq. (2) with the metrics replaced by the components of the cell-face area vectors. The preceding discretization results in either an explicit or implicit algorithm depending on whether the fluxes are evaluated at the n or $n+1$ marching step, respectively. In the present code, the vector $\hat{E}_i$ is defined by

$$(\hat{E}_i)^n_{k,\ell} = \hat{E}^*(\mathrm{d}\boldsymbol{S}^n_{k,\ell},\ \boldsymbol{U}^n_{k,\ell}) + \hat{E}^P(\mathrm{d}\boldsymbol{S}^n_{k,\ell},\ \boldsymbol{U}^{n-1}_{k,\ell}) \tag{15}$$

where the forms of $\hat{E}^*$ and $\hat{E}^P$ are given by Eq. (10), and $\mathrm{d}\boldsymbol{S}^n_{k,\ell}$ and $\boldsymbol{U}^n_{k,\ell}$ indicate the location where the geometry and the physical variables (including ω), respectively, are evaluated.

To avoid the difficulty of extracting the required flow properties from the flux vector $\hat{E}^*$, and to simplify the application of the implicit algorithm, a change is made in the dependent variable from $\hat{E}^*$ to the vector of conserved variables $\boldsymbol{U}$, through the following linearization

$$\hat{E}^*(\mathrm{d}\boldsymbol{S}^n,\ \boldsymbol{U}^n) = \hat{\boldsymbol{A}}^{*n-1}\boldsymbol{U}^n \tag{16}$$

where

$$\boldsymbol{U} = [\rho,\ \rho u,\ \rho v,\ \rho w,\ E_t]^T \tag{17}$$

and

$$\hat{\boldsymbol{A}}^{*n-1} = \frac{\partial \hat{E}^*(\mathrm{d}\boldsymbol{S}^n,\ \boldsymbol{U}^{n-1})}{\partial \boldsymbol{U}^{n-1}} \tag{18}$$

The flux vector $\hat{E}^*$ can be written in the following functional form for a real gas

$$\hat{E}^* = \hat{E}^*(\mathrm{d}\boldsymbol{S},\ \boldsymbol{U},\ \bar{\gamma}) \tag{19}$$

Thus, the Jacobian $\hat{\boldsymbol{A}}^*$ is given by

$$\hat{\boldsymbol{A}}^* = \left(\frac{\partial \hat{E}^*}{\partial \boldsymbol{U}}\right)_{\bar{\gamma}} + \left(\frac{\partial \hat{E}^*}{\partial \bar{\gamma}}\right)_U \left(\frac{\partial \bar{\gamma}}{\partial \boldsymbol{U}}\right) \tag{20}$$

where $(\ )_{\bar{\gamma}}$ and $(\ )_U$ indicate that $\bar{\gamma}$ and $\boldsymbol{U}$ are held constant. Using the correlation $\bar{\gamma} = \bar{\gamma}(\tilde{e},\tilde{\rho})$, the Jacobian can be further expanded as

$$\hat{\boldsymbol{A}}^* = \left(\frac{\partial \hat{E}^*}{\partial \boldsymbol{U}}\right)_{\bar{\gamma}} + \left(\frac{\partial \hat{E}^*}{\partial \bar{\gamma}}\right)_U \left[\tilde{\rho}_\infty \left(\frac{\partial \bar{\gamma}}{\partial \tilde{\rho}}\right)_{\tilde{e}} \left(\frac{\partial \rho}{\partial \boldsymbol{U}}\right) + \tilde{V}^2_\infty \left(\frac{\partial \bar{\gamma}}{\partial \tilde{e}}\right)_{\tilde{\rho}} \left(\frac{\partial e}{\partial \boldsymbol{U}}\right)\right] \tag{21}$$

The parameter ω is assumed locally independent of $\boldsymbol{U}$ and $\bar{\gamma}$ in determining the matrix $(\partial \hat{E}^*/\partial \boldsymbol{U})_{\bar{\gamma}}$. This matrix is given in Ref. 35. The vector $(\partial \hat{E}^*/\partial \bar{\gamma})_U$ can be written as

$$\left(\frac{\partial \hat{E}^*}{\partial \bar{\gamma}}\right)_U = \rho e\left[0,\ \omega\left(\frac{\xi_x}{J}\right),\ \omega\left(\frac{\xi_y}{J}\right),\ \omega\left(\frac{\xi_z}{J}\right),\ \hat{U}\right]^T \tag{22}$$

and the row vectors $\partial\rho/\partial \boldsymbol{U}$ and $\partial e/\partial \boldsymbol{U}$ become

$$\frac{\partial \rho}{\partial \boldsymbol{U}} = [1,\ 0,\ 0,\ 0,\ 0] \tag{23}$$

$$\frac{\partial e}{\partial \boldsymbol{U}} = \frac{1}{\rho}\left[-e + \frac{u^2+v^2+w^2}{2},\ -u,\ -v,\ -w,\ 1\right] \tag{24}$$

For a real gas, the derivatives $(\partial\bar{\gamma}/\partial\tilde{\rho})_{\tilde{e}}$ and $(\partial\bar{\gamma}/\partial\tilde{e})_{\tilde{\rho}}$ can be obtained directly from the curve fit expression used by Srinivasan et al.[30] for $\tilde{a} = \tilde{a}(\tilde{e},\tilde{\rho})$.

After substituting Eqs. (15–18) into Eq. (14), the discretized conservation law takes the form

$$\hat{\boldsymbol{A}}^{*n}_{k,\ell}\delta^{n+1}\boldsymbol{U}_{k,\ell} = -(\hat{\boldsymbol{A}}^{*n}_{k,\ell} - \hat{\boldsymbol{A}}^{*n-1}_{k,\ell})\boldsymbol{U}^n_{k,\ell}$$
$$- \left[(\hat{F}_i - \hat{F}^*_v)^{n+\frac{1}{2}}_{k+\frac{1}{2},\ell} - (\hat{F}_i - \hat{F}^*_v)^{n+\frac{1}{2}}_{k-\frac{1}{2},\ell}\right]$$
$$- \left[(\hat{G}_i - \hat{G}^*_v)^{n+\frac{1}{2}}_{k,\ell+\frac{1}{2}} - (\hat{G}_i - \hat{G}^*_v)^{n+\frac{1}{2}}_{k,\ell-\frac{1}{2}}\right]$$
$$- \left[\hat{E}^p(\mathrm{d}\boldsymbol{S}^{n+1}_{k,\ell},\ \boldsymbol{U}^n_{k,\ell}) - \hat{E}^p(\mathrm{d}\boldsymbol{S}^n_{k,\ell},\ \boldsymbol{U}^{n-1}_{k,\ell})\right] \tag{25}$$

where

$$\delta^{n+1}\boldsymbol{U} = \boldsymbol{U}^{n+1} - \boldsymbol{U}^n$$

At this level, the algorithm is no different than the standard (i.e., Beam-Warming) PNS solver. Where the new algorithm distinguishes itself is in the manner in which the numerical fluxes $\hat{F}$ and $\hat{G}$ are specified. In the definition of the inviscid portions of these fluxes, the algorithm is analogous to the scheme proposed by Roe[22] for solving the Euler equations. Roe's scheme belongs to the subclass of upwind schemes referred to as Riemann solvers that, as the name implies, depend on solutions to Riemann problems in the specification of the numerical fluxes. Rather than solving true Riemann problems, however, Roe's scheme uses solutions to approximate (linearized) Riemann problems, and this considerably simplifies the numerical algorithm. Each of the fluxes, $\hat{F}$ and $\hat{G}$, are evaluated separately by splitting the two-dimensional, linearized Riemann problem into two, one-dimensional, linearized Riemann problems of the following form

$$\frac{\partial \hat{E}^*}{\partial \xi} + D_{m+\frac{1}{2}}\frac{\partial \hat{E}^*}{\partial \kappa} = 0 \qquad (\kappa = \eta \text{ or } \zeta) \tag{26}$$

with initial conditions

$$(\hat{E}^*)^n = \begin{cases} \hat{E}^*(\mathrm{d}\boldsymbol{S}_{m+\frac{1}{2}},\ \boldsymbol{U}_{m+1}) & \kappa > \kappa_{m+\frac{1}{2}} \\ \hat{E}^*(\mathrm{d}\boldsymbol{S}_{m+\frac{1}{2}},\ \boldsymbol{U}_m) & \kappa < \kappa_{m+\frac{1}{2}} \end{cases} \tag{27}$$

for the $m + \frac{1}{2}$ cell interface. The matrix $D_{m+\frac{1}{2}}$ is of the form

$$D_{m+\frac{1}{2}} = \left(\frac{\kappa_x}{J}\right)_{m+\frac{1}{2}} \left(\frac{\partial E_i}{\partial \hat{E}^*}\right)_{m+\frac{1}{2}} + \left(\frac{\kappa_y}{J}\right)_{m+\frac{1}{2}} \left(\frac{\partial F_i}{\partial \hat{E}^*}\right)_{m+\frac{1}{2}} + \left(\frac{\kappa_z}{J}\right)_{m+\frac{1}{2}} \left(\frac{\partial G_i}{\partial \hat{E}^*}\right)_{m+\frac{1}{2}} \tag{28}$$

In spite of the nonconservative form of Eq. (26), the local shock capturing capabilities of the algorithm can be retained if the flow properties making up $D_{m+\frac{1}{2}}$ are carefully averaged between the grid points m and $m+1$ to satisfy the relation

$$D_{m+\frac{1}{2}}\left[\hat{E}^*(\mathrm{d}S^n_{m+\frac{1}{2}},\ U^n_{m+1}) - \hat{E}^*(\mathrm{d}S^n_{m+\frac{1}{2}},\ U^n_m)\right] = (\kappa_x/J)_{m+\frac{1}{2}}\Delta E_i + (\kappa_y/J)_{m+\frac{1}{2}}\Delta F_i + (\kappa_z/J)_{m+\frac{1}{2}}\Delta G_i \tag{29}$$

For an inviscid supersonic flow of a *perfect* gas, Roe has suggested a procedure for finding $D_{m+\frac{1}{2}}$ that satisfies Eq. (29). For equilibrium calculations, γ is no longer a constant but depends upon the thermodynamic state of the gas, and the procedure of Ref. 22 can no longer be used to determine $D_{m+\frac{1}{2}}$. For this case, Grossman and Walters[25] have developed an approximate procedure for finding $D_{m+\frac{1}{2}}$. More recently, Vinokur and Liu[28] have presented a more exact method for determining $D_{m+\frac{1}{2}}$. In the present study, the method of Vinokur and Liu has been adapted to the three-dimensional PNS equations.

The approach of Vinokur and Liu yields the same Roe-averaged variables as the perfect gas analysis for the three velocity components (u, v, and w) and the total enthalpy ($H = e + p/\rho + \frac{1}{2}V^2$). The momentum equation gives rise to the following new relationship, which must also be satisfied.

$$\Delta p = \bar{\chi}\Delta\rho + \bar{K}\Delta(\rho e) \tag{30}$$

where

$$\chi = \left(\frac{\partial p}{\partial \rho}\right)_{\rho e} \tag{31a}$$

$$K = \left(\frac{\partial p}{\partial(\rho e)}\right)_{\rho} \tag{31b}$$

and $\bar{\chi}$ and $\bar{K}$ are some averaged values of χ and K. Equation (30) is simply the discrete form of the differential of the pressure, and is exactly satisfied for a perfect gas. The derivatives χ and K can be expressed as follows

$$\chi = \rho e\left(\frac{\partial \bar{\gamma}}{\partial \rho}\right)_e - e^2\left(\frac{\partial \bar{\gamma}}{\partial e}\right)_\rho \tag{32a}$$

$$K = (\bar{\gamma} - 1) + e\left(\frac{\partial \bar{\gamma}}{\partial e}\right)_\rho \tag{32b}$$

For a perfect gas, these terms reduce to $\chi = 0$ and $K = (\gamma_\infty - 1)$. Equation (30) is the only relation between the variables $\bar{\chi}$ and $\bar{K}$, and a simple average of the left and right states of χ and K will not, in general, satisfy this relation. However, Vinokur and Liu have arrived at a particular form of averaging the variables χ and K that will satisfy Eq. (30) in the general case. The averaging takes the following form:

$$\frac{1}{\bar{K}} = \frac{D\Delta\rho + \Delta p\Delta(\rho e)}{[(\Delta p)^2 + \hat{a}^4(\Delta\rho)^2]} \tag{33a}$$

$$\frac{\bar{\chi}}{\bar{K}} = \frac{D\Delta p - \hat{a}^4\Delta\rho\Delta(\rho e)}{[(\Delta p)^2 + \hat{a}^4(\Delta\rho)^2]]} \tag{33b}$$

where

$$D = \tfrac{1}{2}\left[\left(\frac{\chi_L}{K_L} + \frac{\chi_R}{K_R}\right)\Delta p + \left(\frac{1}{K_L} + \frac{1}{K_R}\right)\hat{a}^4\Delta\rho\right] \tag{34a}$$

$$\hat{a}^2 = \tfrac{1}{2}\left[(a_L)^2 + (a_R)^2\right] \tag{34b}$$

and the subscripts L and R represent the left and right states. Other forms of averaging are possible; however, this is the form that was used in the present study. In the freestream, simple averages are used for $\bar{\chi}$ and $\bar{K}$.

Once $\bar{\chi}$ and $\bar{K}$ have been determined, the Roe-averaged speed of sound $\bar{a}$ is defined as

$$\bar{a} = \bar{\chi} + \bar{K}\bar{h} \tag{35}$$

where $\bar{h}$ is the specific enthalpy obtained from Roe-averaged quantities in the following manner

$$\bar{h} = \bar{H} - \tfrac{1}{2}(\bar{u}^2 + \bar{v}^2 + \bar{w}^2) \tag{36}$$

The solution to the preceding approximate Riemann problem consists of four constant-property regions separated by three surfaces of discontinuity emanating from the cell edge (ξ^n, $\kappa_{m+\frac{1}{2}}$) and having slopes given by the eigenvalues of $D_{m+\frac{1}{2}}$. Of particular interest to the numerical algorithm is the resulting flux across the $m + \frac{1}{2}$ cell interface. This first-order-accurate inviscid flux consists of an unbiased component plus

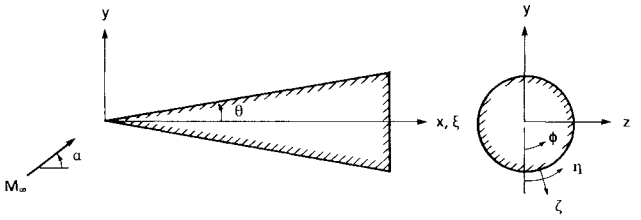

Fig. 1 Coordinate system.

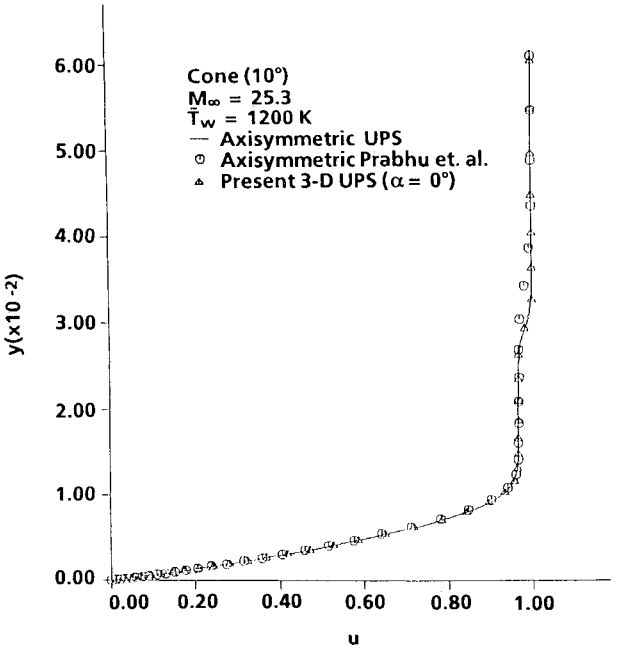

Fig. 2 Comparison of velocity profiles at $\bar{x} = 1$ m.

a first-order upwind dissipation term and is given by

$$\hat{H}^1_{m+\frac{1}{2}} = \left(\frac{\kappa_x}{J}\right)_{m+\frac{1}{2}} \tfrac{1}{2}[(E_i)_m + (E_i)_{m+1}] + \left(\frac{\kappa_y}{J}\right)_{m+\frac{1}{2}} \tfrac{1}{2}[(F_i)_m + (F_i)_{m+1}] + \left(\frac{\kappa_z}{J}\right)_{m+\frac{1}{2}} \tfrac{1}{2}[(G_i)_m + (G_i)_{m+1}] - \tfrac{1}{2}(\text{sgn } D)_{m+\frac{1}{2}} \left[\left(\frac{\kappa_x}{J}\right)_{m+\frac{1}{2}} \Delta E_i + \left(\frac{\kappa_y}{J}\right)_{m+\frac{1}{2}} \Delta F_i + \left(\frac{\kappa_z}{J}\right)_{m+\frac{1}{2}} \Delta G_i\right] \tag{37}$$

In this equation, the matrix sgn D is defined as

$$\text{sgn } D = R(\text{sgn } \Lambda)R^{-1} \tag{38}$$

where R is the matrix of right eigenvectors and sgn Λ is the diagonal matrix that has elements

$$\text{sgn } \lambda^i = \frac{\lambda^i}{|\lambda^i|} \tag{39}$$

and Δ is the standard forward difference operator. The real-gas eigenvalues and eigenvectors are given in Ref. 35.

First-order inviscid numerical fluxes in the η and ζ directions are then given by

$$(\hat{F}^1_i)_{k+\frac{1}{2},\ell} = \hat{H}^1_{k+\frac{1}{2},\ell}, \qquad (\hat{G}^1_i)_{k,\ell+\frac{1}{2}} = \hat{H}^1_{k,\ell+\frac{1}{2}} \tag{40}$$

respectively. The flux in the η direction, $\hat{H}_{k+\frac{1}{2},\ell}$, is obtained by inserting η for κ and $k+\frac{1}{2},\ell$ for $m+\frac{1}{2}$. Likewise, the flux in the ζ direction, $\hat{H}_{k,\ell+\frac{1}{2}}$, is obtained by replacing κ with ζ and $m+\frac{1}{2}$ with $k,\ell+\frac{1}{2}$. Viscous stresses and heat-transfer fluxes are evaluated in both crossflow directions using a standard central-differencing approach.

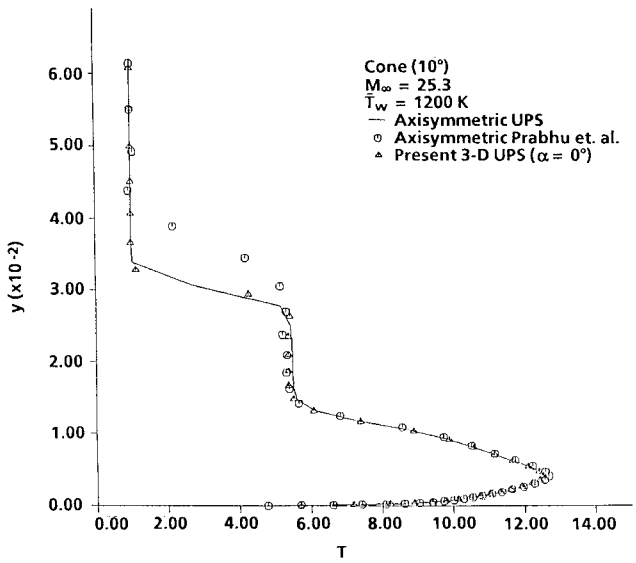

Fig. 3 Comparison of temperature profiles at $\tilde{x} = 1$ m.

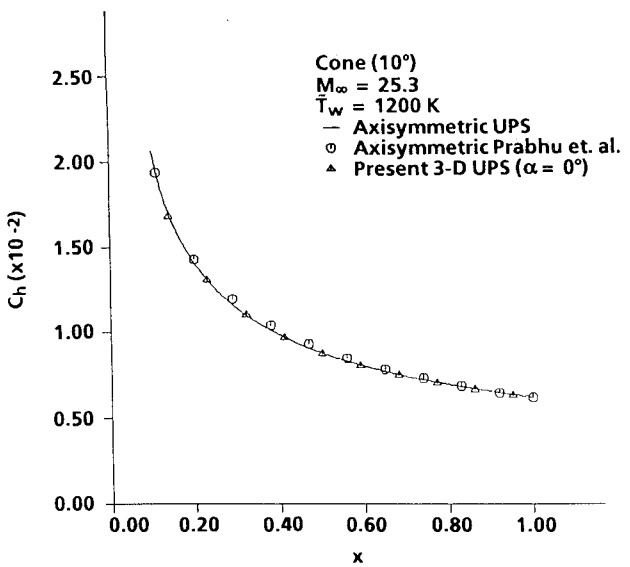

Fig. 5 Comparison of heat transfer coefficients.

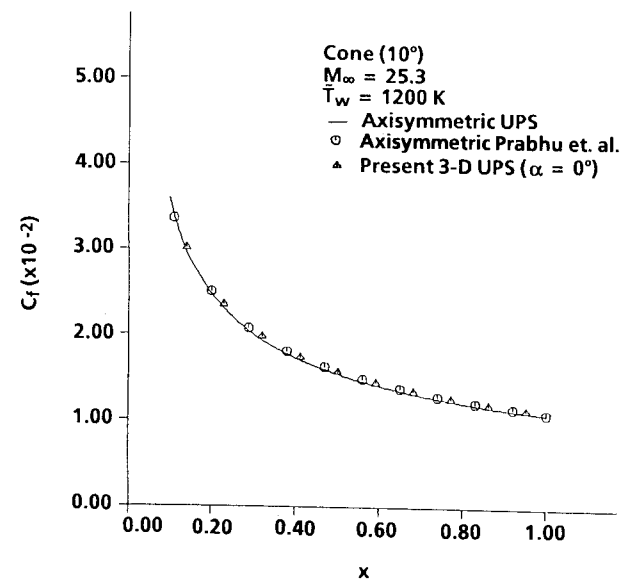

Fig. 4 Comparison of skin friction coefficients.

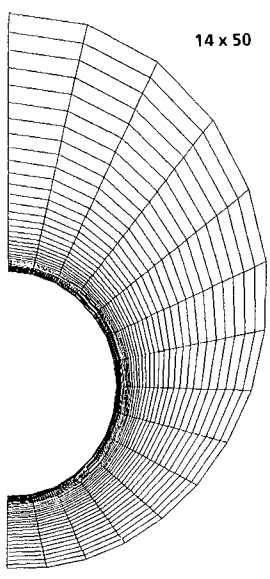

Fig. 6 Computational grid, $\alpha = 10$ deg.

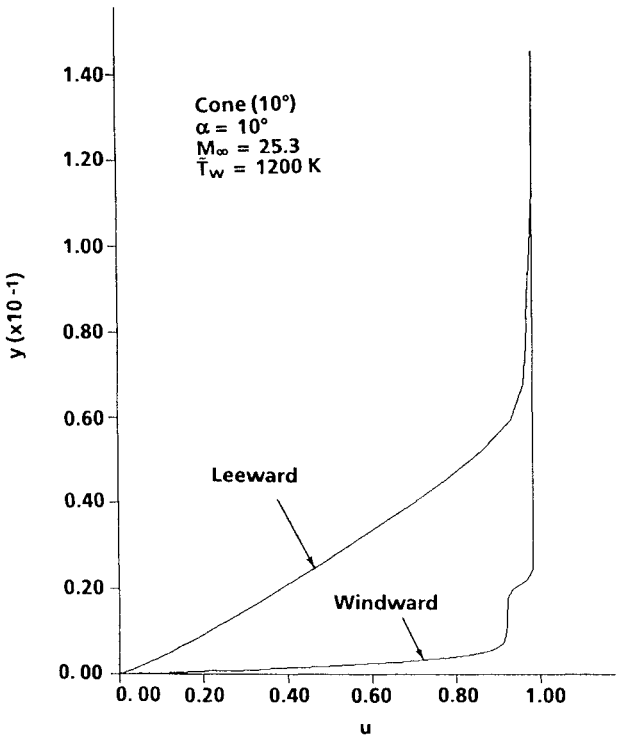

Fig. 7 Windward and leeward velocity profiles at $\bar{x} = 1$ m.

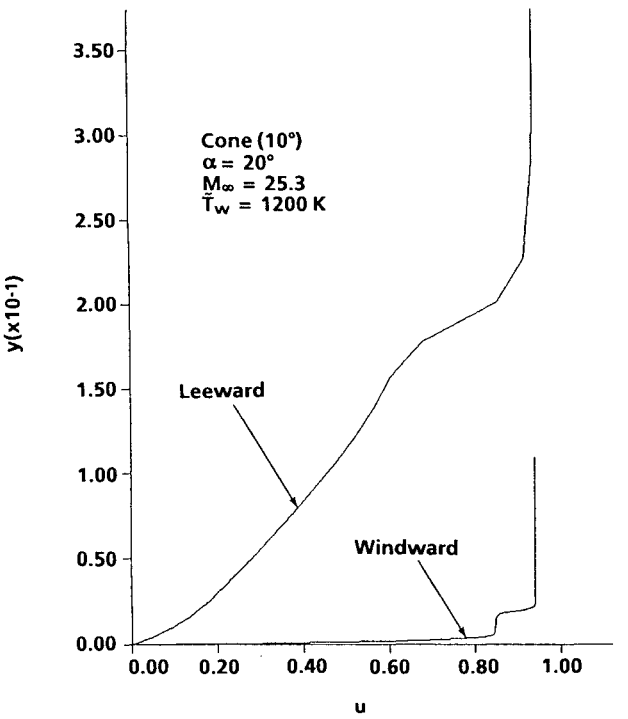

Fig. 9 Windward and leeward velocity profiles at $\bar{x} = 1$ m.

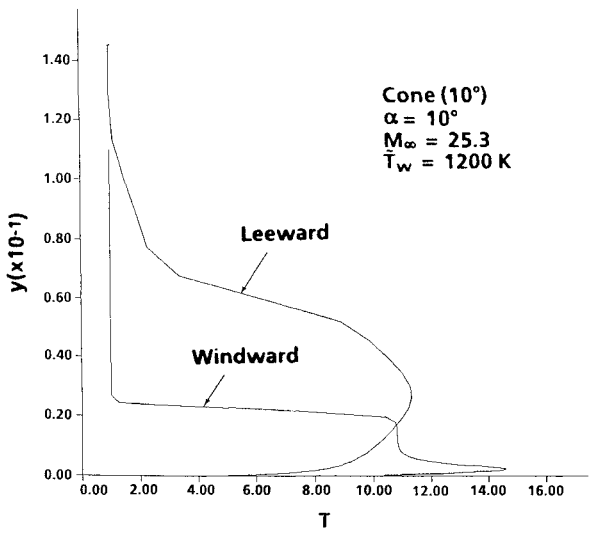

Fig. 8 Windward and leeward temperature profiles at $\bar{x} = 1$ m.

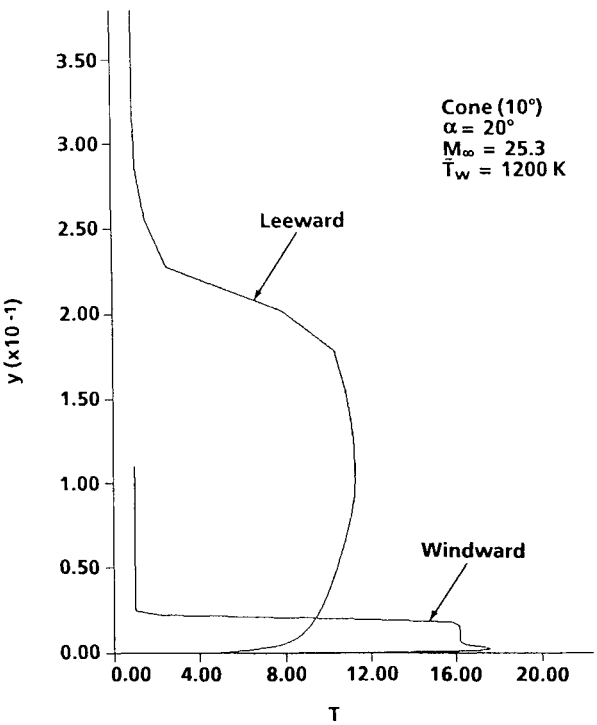

Fig. 10 Windward and leeward temperature profiles at $\bar{x} = 1$ m.

The first-order, real-gas, upwind algorithm described previously is upgraded to second-order accuracy in the η and ζ directions using an approach similar to the one employed by Chakravarthy and Szema[36] for the unsteady Euler equations. In addition, the present algorithm is made implicit by evaluating the numerical fluxes at the $n+1$ marching station. The flux terms are linearized to produce a block tridiagonal system of equations, which can be solved in a relatively efficient manner. Further details of the numerical algorithm can be found in Ref. 21.

Numerical Results

The new three-dimensional, real-gas, upwind PNS code has been used to compute high Mach number flows of equilibrium air over cones at various angles of attack. The results of these computations are compared with the results from a conventional centrally differenced, real-gas PNS code developed by Prabhu et al.[3,12] and the previous axisymmetric, upwind, real-gas PNS code.[23]

Test Case I

The first test case consists of the $M_\infty = 25$ laminar flow of equilibrium air over a 10-deg, half-angle cone at 0-, 10-, and 20-deg angles of attack. The flow conditions for this test case match those used by Prabhu et al. and correspond to an altitude of 60.96 km where the ambient pressure and temperature are 20.35 N/m^2 and 252.6 K, respectively. The other pertinent

flow parameters are

$$M_\infty = 25.3, \qquad Re_\infty = 1.29 \times 10^5, \qquad Pr_\infty = 0.72$$

$$\tilde{T}_w = 1200 \text{ K}, \qquad \gamma_\infty = 1.4 \tag{41}$$

The coordinate system for this test case is shown in Fig. 1. The grid for the 0- and 10-deg angle of attack calculations contained 50 cells in the normal direction and 14 cells in the circumferential direction. The grid for the 20-deg angle of attack calculation was 50×29 cells. The height of the first cell above the cone surface was specified as 1×10^{-4} m, and this value was used to determine the appropriate Roberts stretching parameter[29] β for the remaining cells. The ξ = constant grid lines were placed normal to the x axis. The initial conditions (at $\tilde{x} = 0.05$ m) were obtained using the conical step-back procedure. The solution was then marched 1900 steps downstream with a 5×10^{-4} m step-size and terminated at $\tilde{x} = 1$ m.

The velocity and temperature profiles at $\tilde{x} = 1$ m are compared in Figs. 2 and 3 for the 0-deg angle of attack case. The present three-dimensional results are compared with the axisymmetric results from the centrally differenced Prabhu et

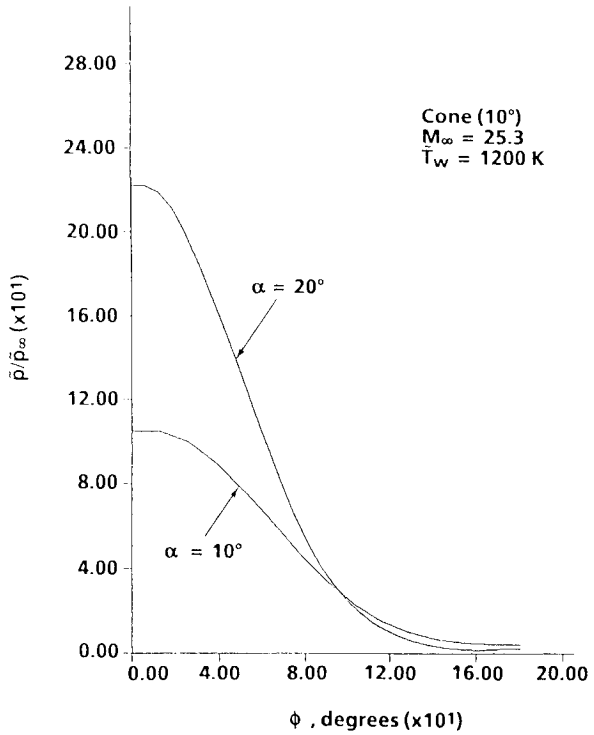

Fig. 11 Circumferential pressure distribution at $\tilde{x} = 1$ m.

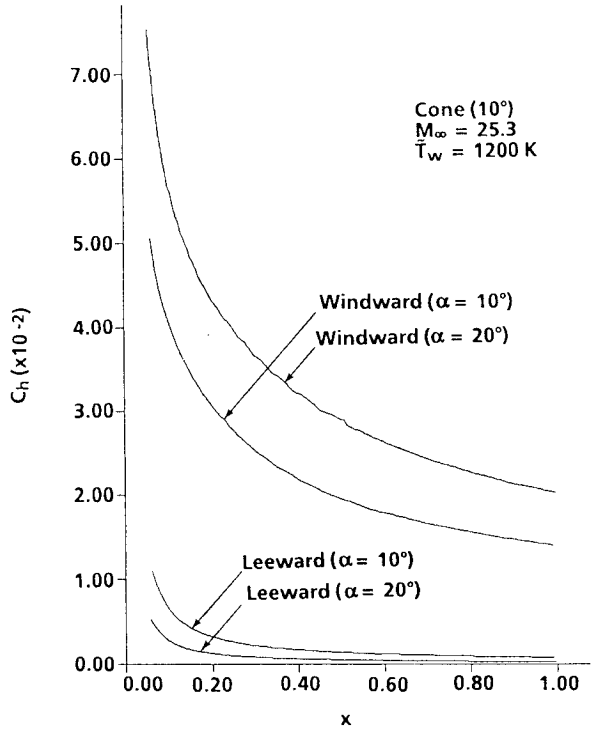

Fig. 13 Stream-wise variation of heat transfer coefficients.

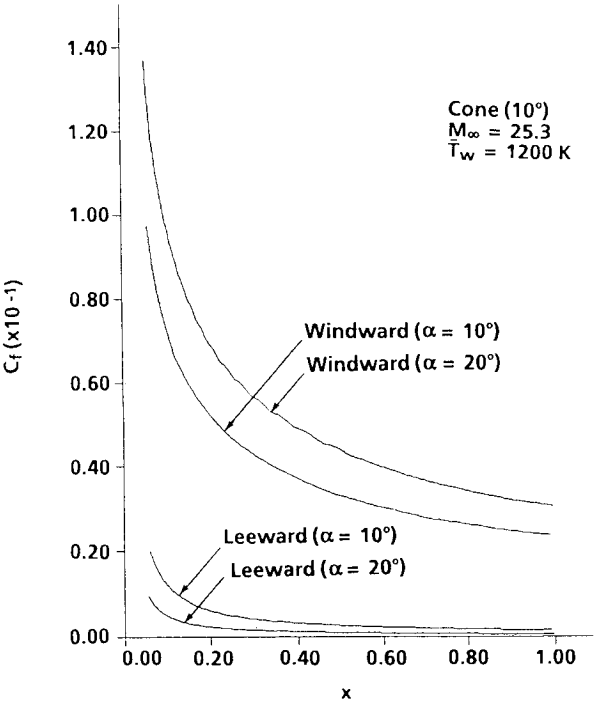

Fig. 12 Stream-wise variation of skin friction coefficients.

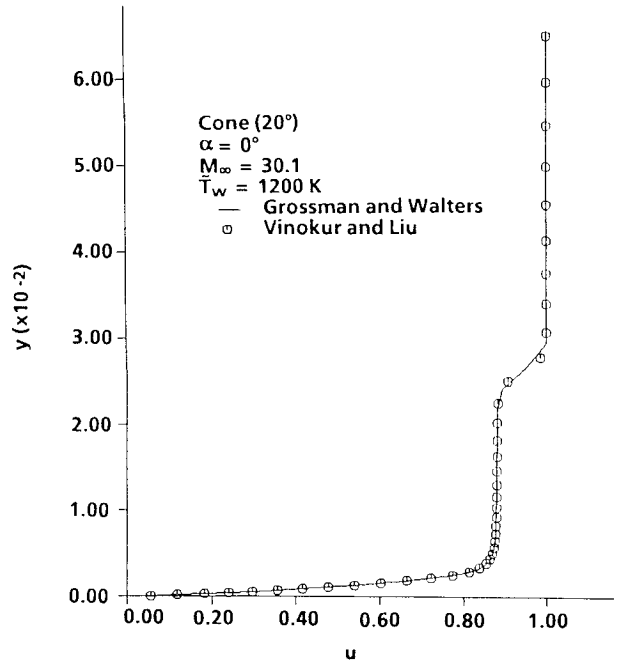

Fig. 14 Comparison of velocity profiles at $\tilde{x} = 1$ m.

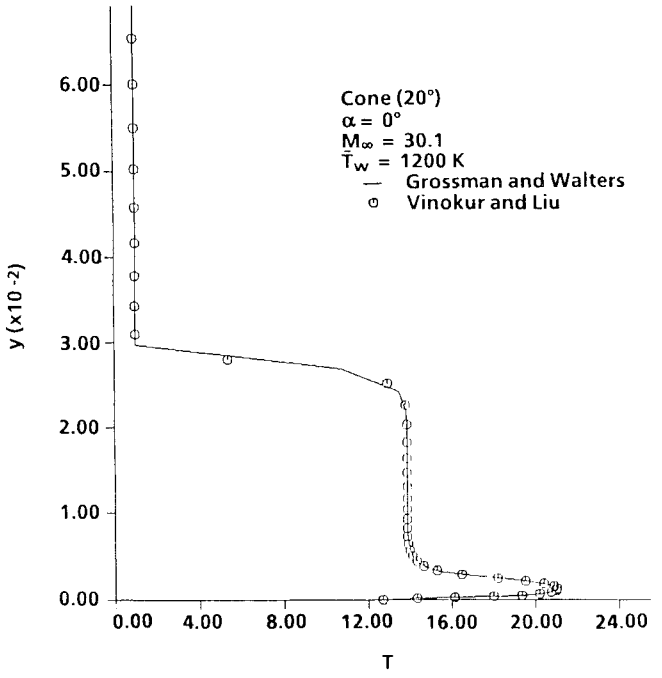

Fig. 15 Comparison of temperature profiles at $\tilde{x} = 1$ m.

al.[3,12] code and the previous upwind, real-gas code.[23] The comparison is excellent except near the bow shock region where the centrally differenced PNS code "smears" the solution over five mesh points, whereas the upwind codes resolve the discontinuity in typically three mesh points. The smearing of the centrally differenced solution is a result of the artificial smoothing necessary to maintain a monotonic profile in the shock region.

Figures 4 and 5 display the stream-wise variations of the coefficients of skin friction and heat transfer. The formulas used to compute these quantities are

$$C_f = \frac{2\mu_w}{Re_\infty}\frac{\partial u}{\partial n} \tag{42}$$

$$C_h = \frac{\mu_w}{Pr_\infty Re_\infty}\left[\frac{(\gamma_\infty - 1)M_\infty^2}{2} + 1 - T_w\right]^{-1}\frac{\partial T}{\partial n} \tag{43}$$

where n represents the distance normal to the wall. For both coefficients, the agreement between the codes is excellent.

The finite-volume grid for the 10-deg angle of attack case is shown in Fig. 6. The present results for the 10- and 20-deg cases are displayed in Figs. 7-13. The windward and leeward profiles of velocity and temperature at $\tilde{x} = 1$ m are shown in Figs. 7-10. The circumferential variation of pressure at $\tilde{x} = 1$ m is shown in Fig. 11. The stream-wise variations of skin friction

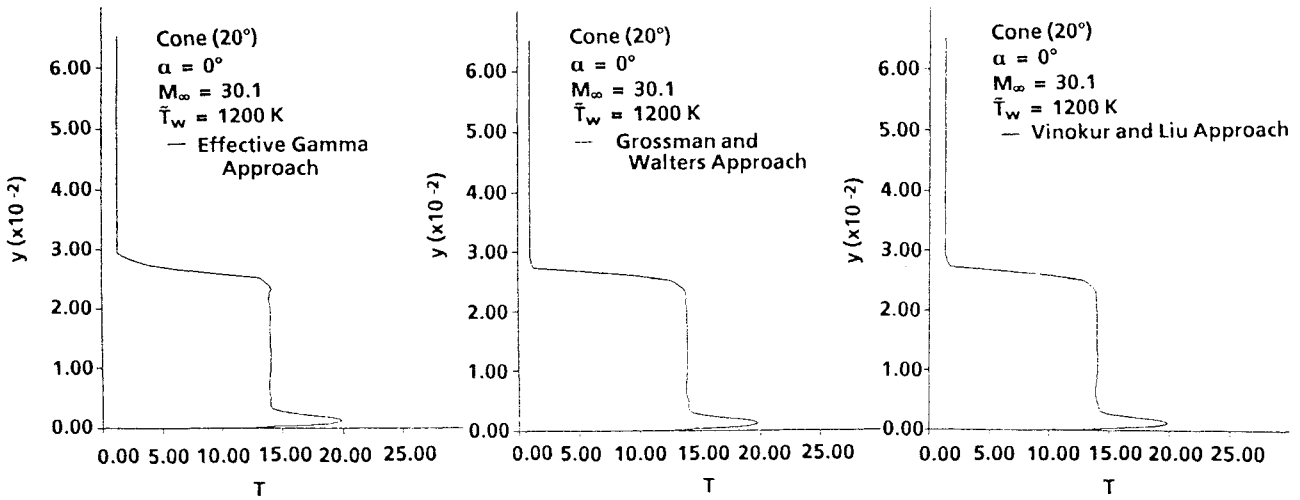

Fig. 16 Comparison of temperature profiles at $\tilde{x} = 1$ m.

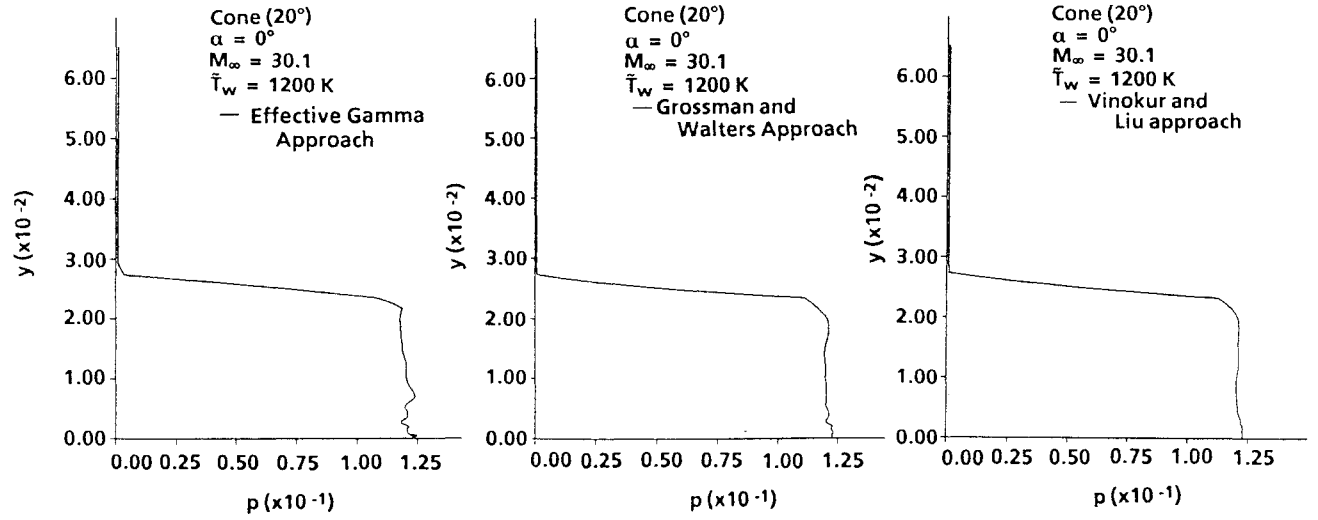

Fig. 17 Comparison of pressure profiles at $\tilde{x} = 1$ m.

and heat transfer on the windward and leeward sides of the cone are given in Figs. 12 and 13. As expected, the skin friction and heat transfer increase with increasing angle of attack on the windward side and decrease with increasing angle of attack on the leeward side.

The small "wiggles" that appear in Figs. 12 and 13 are due to the performance of the shock capturing scheme, which captures shocks with two to three interior points. As the shock wave moves oblique to the nearly aligned grid, it "jumps" from one grid line to the next. This spawns nonphysical waves (in severe cases only) that propagate toward the body surface causing small oscillations to appear in the stream-wise plots of skin friction and heat transfer.

Test Case II

The second test case was used to compare the approach of Vinokur and Liu with the approximate approaches of Grossman and Walters and the simple "effective gamma" method. The test case consists of the $M_\infty = 30$ laminar flow of equilibrium air over a 20-deg half-angle cone at 0-deg angle of attack. The flow conditions correspond to an altitude of 30.48 km and are given by

$$M_\infty = 30.1, \qquad Re_\infty = 9.08 \times 10^5, \qquad Pr_\infty = 0.72$$

$$\tilde{T}_w = 1200 \text{ K}, \qquad \gamma_\infty = 1.4 \tag{44}$$

These conditions lead to large gradients in the flowfield and were purposely chosen to emphasize the differences among the three approaches. The finite-volume grid used for this three-dimensional calculation consisted of 50 cells in the normal direction and 14 cells in the circumferential direction.

The velocity and temperature profiles at $\tilde{x} = 1$ m are compared in Figs. 14 and 15 for the Vinokur and Liu and Grossman and Walters approaches. Only small differences can be detected between the two approaches. A comparison of the temperature profiles at $\tilde{x} = 1$ m is shown in Fig. 16 for all three approaches. The effective gamma approach produces a shock that is not as "sharp" as the shocks given by the other two methods. Furthermore, a small oscillation in the profile can be seen downstream of the shock. A comparison of the pressure profiles at $\tilde{x} = 1$ m is shown in Fig. 17. Pressure oscillations are evident in both the effective gamma approach and the Grossman and Walters approach. These oscillations are not present in the Vinokur and Liu approach.

All of the present computations were performed on an Apollo DN3000 workstation. The three-dimensional upwind, real-gas PNS code requires 0.146 s/step/cell of computer time using the Vinokur and Liu approach and 0.139 s/step/cell using the Grossman and Walters approach.

Concluding Remarks

A new real-gas, upwind, PNS code has been developed to compute the three-dimensional hypersonic flow of equilibrium air. The code has been used to compute the $M_\infty = 25$ laminar flow of air over a 10-deg, half-angle cone at 0-, 10-, and 20-deg angles of attack. The results of these computations are in excellent agreement with those obtained using a centrally differenced, real-gas PNS code, except in the vicinity of the shock wave, where the present code is clearly superior in resolving the discontinuity. The Vinokur and Liu approach was shown to be clearly superior to the effective gamma approach but gave only a slight improvement over the Grossman and Walters approach. The present three-dimensional equilibrium code has recently been extended to permit finite-rate chemically reacting flows to be computed.

Acknowledgments

This work was supported by the NASA Ames Research Center through a Small Business Innovation Research (SBIR) Contract (NAS2-12861). The Technical Monitor for this contract is Dr. Terry L. Holst.

References

[1]Li, C. P., "Numerical Simulation of Re-Entry Flow Around the Space Shuttle Orbiter Including Real Gas Effects," *Computers in Flow Predictions and Fluid Dynamics Experiments,* American Society of Mechanical Engineers, New York, Nov. 1981, pp. 141-149.

[2]Gnoffo, P. A., "Hypersonic Flows Over Biconics Using a Variable-Effective-Gamma Parabolized-Navier-Stokes Code," AIAA Paper 83-1666, July 1983.

[3]Prabhu, D. K., and Tannehill, J. C., "Numerical Solution of Space Shuttle Orbiter Flow Field Including Real Gas Effects," AIAA Paper 84-1747, June 1984; also *Journal of Spacecraft and Rockets,* Vol. 23, No. 3, 1986, pp. 264-272.

[4]Bhutta, B. A., Lewis, C. H., and Kautz, F. A., II, "Hypersonic Equilibrium-Air Flows Using an Implicit Non-Iterative Parabolized Navier-Stokes Scheme," AIAA Paper 85-0169, Jan. 1985.

[5]Banken, G. J., Roberts, D. W., Holcomb, J. E., and Birch, S. R., "An Investigation of Film Cooling on a Hypersonic Vehicle Using a PNS Flow Analysis Code," AIAA Paper 85-1591, July 1985.

[6]Molvik, G. A., "A Parabolized Navier-Stokes Code with Real Gas Effects," 1985 Parabolized N-S Code Workshop, Wright-Patterson AFB, Sept. 1985.

[7]Stalnaker, J. F., Nicholson, L. A., Hauline, D. S., and McGraw, E. H., "Improvements to the AFWAL PNS Code Formulation," AFWAL-TR-86-3076, Sept. 1976.

[8]Liou, M.-F., "Three Dimensional PNS Solutions of Hypersonic Internal Flows with Equilibrium Chemistry," AIAA Paper 89-0002, Jan. 1989.

[9]Bhutta, B. A., Lewis, C. H., and Kautz, F. A., II, "A Fast Fully-Iterative Parabolized Navier-Stokes Scheme for Chemically-Reacting Reentry Flows," AIAA Paper 85-0926, June 1985.

[10]Sinha, N., and Dash, S. M., "Parabolized Navier-Stokes Analysis of Ducted Turbulent Mixing Problems with Finite-Rate Chemistry," AIAA Paper 86-0004, Jan. 1986.

[11]Prabhu, D. K., Tannehill, J. C., and Marvin, J. G., "A New PNS Code for Chemical Nonequilibrium Flows," AIAA Paper 87-0248, Jan. 1987; also *AIAA Journal,* Vol. 26, No. 7, 1988, pp. 808-815.

[12]Prabhu, D. K., Tannehill, J. C., and Marvin, J. G., "A New PNS Code for Three-Dimensional Chemically Reacting Flows," AIAA Paper 87-1472, June 1987.

[13]Sinha, N., Dash, S. M., and Krawczyk, W. J., "Inclusion of Chemical Kinetics into Beam-Warming Based PNS Model for Hypersonic Propulsion Applications," AIAA Paper 87-1898, June-July 1987.

[14]Gielda, T. P., Hunter, L. G., and Chawner, J. R., "Efficient Parabolized Navier-Stokes Solutions of Three-Dimensional, Chemically Reacting Scramjet Flowfields," AIAA Paper 88-0096, Jan. 1988.

[15]Chitsomboon, T., and Northam, G. B., "A 3D-PNS Computer Code for the Calculation of Supersonic Combusting Flows," AIAA Paper 88-0438, Jan. 1988.

[16]Gielda, T. P., and Agarwal, R. K., "Efficient Finite-Volume Parabolized Navier-Stokes Solutions for Three-Dimensional, Hypersonic, Chemically Reacting Flowfields," AIAA Paper 89-0103, Jan. 1989.

[17]Molvik, G. A., and Merkle, C. L., "A Set of Strongly Coupled Upwind Algorithms for Computing Flows in Chemical Nonequilibrium," AIAA Paper 89-0199, Jan. 1989.

[18]Kamath, H., "Parabolized Navier-Stokes Algorithm for Chemically Reacting Flows," AIAA Paper 89-0386, Jan. 1989.

[19]Beam, R., and Warming, R. F., "An Implicit Factored Scheme for the Compressible Navier-Stokes Equations," *AIAA Journal,* Vol. 16, April 1978, pp. 393-401.

[20]Lawrence, S. L., Tannehill, J. C., and Chaussee, D. S., "An Upwind Algorithm for the Parabolized Navier-Stokes Equations," AIAA Paper 86-1117, May 1986.

[21]Lawrence, S. L., Chaussee, D. S., and Tannehill, J. C., "Application of an Upwind Algorithm to the Three-Dimensional Parabolized Navier-Stokes Equations," AIAA Paper 87-1112, June 1987.

[22]Roe, P. L., "Approximate Riemann Solvers, Parameter Vectors, and Difference Schemes," *Journal of Computational Physics,* Vol. 43, 1981, pp. 357-372.

[23]Tannehill, J. C., Ievalts, J. O., and Lawrence, S. L., "An Upwind Parabolized Navier-Stokes Code for Real Gas Flows," AIAA Paper 88-0713, Jan. 1988.

[24]Tannehill, J. C., Ievalts, J. O., Prabhu, D. K., and Lawrence, S. L., "An Upwind Parabolized Navier-Stokes Code for Chemically Reacting Flows," AIAA Paper 88-2614, June 1988.

[25]Grossman, B., and Walters, R. W., "An Analysis of Flux-Split Algorithms for Euler's Equations with Real Gases," *Proceedings of the AIAA 8th Computational Fluid Dynamics Conference,* AIAA, New York, 1987, pp. 177-186.

[26]Colella, P., and Glaz, P. M., "Efficient Solution Algorithms for the Riemann Problem for Real Gases," *Journal of Computational Physics,* Vol. 59, 1985, pp. 264–289.

[27]Balakrishnan, A., and Lawrence, S. L., "Equilibrium Air Modifications to UPS and CNS Codes," Workshop on Ames Hypersonic CFD Codes, NASA Ames Research Center, Aug. 1988.

[28]Vinokur, M., and Liu, Y., "Equilibrium Gas Flow Computations II: An Analysis of Numerical Formulations of Conservation Laws," AIAA Paper 88-0127, Jan. 1988.

[29]Anderson, D. A., Tannehill, J. C., and Pletcher, R. H., *Computational Fluid Mechanics and Heat Transfer,* Hemisphere, New York, 1984, pp. 431–432.

[30]Srinivasan, S., Tannehill, J. C., and Weilmuenster, K. J., "Simplified Curve Fits for the Thermodynamic Properties of Equilibrium Air," NASA RP-1181, Aug. 1987.

[31]Srinivasan, S., Tannehill, J. C., and Weilmuenster, K. J., "Simplified Curve Fits for the Transport Properties of Equilibrium Air," NASA CR-178411, Dec. 1987.

[32]Peng, T. C., and Pindroh, A. L., "An Improved Calculation of Gas Properties at High Temperatures: Air," The Boeing Co., Seattle, WA, Rept. D2-11722, 1962.

[33]Anderson, J. D., *Hypersonic and High Temperature Gas Dynamics,* McGraw-Hill, New York, 1989, pp. 603–604.

[34]Vigneron, Y. C., Rakich, J. V., and Tannehill, J. C., "Calculation of Supersonic Viscous Flow Over Delta Wings with Sharp Subsonic Leading Edges," AIAA Paper 78-1137, July 1978.

[35]Tannehill, J. C., Buelow, P. E., Ievalts, J. O., and Lawrence, S. L., "A Three-Dimensional Upwind Parabolized Navier-Stokes Code for Real Gas Flows," AIAA Paper 89-1651, June 1989.

[36]Chakravarthy, S. R. and Szema, K. Y., "An Euler Solver for Three-Dimensional Supersonic Flows with Subsonic Pockets," AIAA Paper 85-1703, July 1985.

Clark H. Lewis
Associate Editor